Pure Appl. Chem., Vol. 85, No. 2, pp. 417–425, 2013.
http://dx.doi.org/10.1351/PAC-CON-12-06-06

Facile solvothermal synthesis of single-crystalline anatase nanorods for efficient dye-sensitized solar cells*

Xiao Wang[1], Feng Hao[1], Huiyuan Chen[2], Gang Wang[2], Jianbao Li[1], and Hong Lin[1,‡]

[1]State Key Laboratory of New Ceramics and Fine Processing, Department of Materials Science and Engineering, Tsinghua University, Beijing 100084, China; [2]Collage of Chemical Engineering, Qinghai University, Xining, Qinghai 810016, China

Abstract: Single-crystalline anatase TiO_2 nanorods (TiO_2-SANRs) were synthesized through a facile solvothermal method and successfully applied as the photoanodes for efficient dye-sensitized solar cells (DSCs). The prepared samples were characterized by scanning electron microscopy (SEM), transmission electron microscopy (TEM), and X-ray diffraction (XRD). The power conversion efficiencies of TiO_2-SANRs decorated Degussa P25 nanoparticle solar cells increased by 13.5 % compared with commercial Degussa P25 TiO_2 solar cells under standard illumination conditions (AM 1.5G, 100 mW/cm^{-2}). The improved performance of the TiO_2-SANRs decorated Degussa P25 nanoparticle solar cells was primarily ascribed to the enhanced short-circuit photocurrent density (J_{sc}) despite a declined dye-loading capacity. The light-scattering effect in the long-wavelength region, as evidenced from the incident photon-to-current conversion efficiency (IPCE) response and the diffuse reflectance spectroscopy was recognized as the main reason for the photocurrent enrichment.

Keywords: anatase; dye-sensitized solar cells (DSCs); light-scattering effects; nanorods; single-crystalline.

INTRODUCTION

Dye-sensitized solar cells (DSCs), mainly based on mesoporous TiO_2 films made from nanocrystalline TiO_2 particles and organic sensitizers, were first reported by Prof. Grätzel in 1991 [1]. With low-cost, high theoretical conversion efficiency, and eco-friendly preparation technology, DSCs have attracted massive interest and been greatly developed through numerous efforts made by various research institutions [2–8]. Efficient functioning of such devices is based on the ultrafast electron injection from the photoexcited state of the dye molecule into the conduction band of the TiO_2, followed by regeneration of the dye with redox couple in the electrolyte. Photoanode materials, the key component of DSCs, have become a hot spot of materials chemistry research [9–12]. Nanocrystalline TiO_2 particles, commonly used in DSCs, provide a large surface area to adsorb efficient dye-loading and therefore light-harvesting performance [13].

Pure Appl. Chem.* **85, 315–462 (2013). A collection of invited papers based on presentations at the 12th Eurasia Conference on Chemical Sciences, Corfu, Greece, 16–21 April 2012.
‡Corresponding author: Tel.: +86 10-62772672; Fax: +86 10-62772672; E-mail: Hong-lin@tsinghua.edu.cn

However, the sizes of TiO_2 nanoparticles commonly applied in DSCs are much smaller than the wavelength of visible light. The film is thus transparent with little light-scattering property. To address this problem, a variety of large-sized TiO_2 nanoparticles (100–400 nm) have been widely employed as light-scattering centers to increase the optical length in the film, and an enhanced light-harvesting performance especially in the long-wavelength region has been demonstrated both experimentally and theoretically [14–19]. Besides these large-sized nanoparticles, various one-dimensional (1D) nanostructures have also been proven to be effective alternatives to enhance the performance of DSCs due to their facilitated electron transport and enhanced the light-harvesting ascribed to the light-scattering effect [20–22]. Recently, we have reported that single-crystalline rutile TiO_2 nanorods evoked an obvious light-scattering effect in the long-wavelength region, which generated a high short-circuit current of 15.62 mA cm^{-2} compared with 13.13 mA cm^{-2} for blank P25 electrode [22]. However, with an almost 0.2 V more positive conduction band edge of the rutile crystal than that of anatase analogue, such rutile TiO_2 nanorods could reduce open-circuit voltage and then affected the overall conversion efficiencies of the devices [22]. More importantly, it is recognized that the electron diffusion coefficient in the rutile crystal is one or two orders lower than its anatase counterpart [23]. Therefore, efforts on the controllable synthesis of the nanosized low-dimensional anatase single crystals possessing both sufficient surface area and light-scattering effect might further promote the photovoltaic conversion efficiency of DSC devices.

In 1998, Kasuga et al. [24] first reported a simple method for the preparation of TiO_2 nanotubes by treatment of amorphous TiO_2 with a concentrated solution of NaOH (10 M) at elevated temperatures. It has since been demonstrated that all polymorphs of TiO_2 (anatase, rutile, brookite, or amorphous forms) can be transformed to the nanotube or nanofiber under alkaline hydrothermal conditions [25–27], and the sample displayed a crystal-phase evolution from $Na_2Ti_3O_7$ to $H_2Ti_2O_5{\cdot}H_2O$ to anatase TiO_2 [28]. When the temperature for the alkaline hydrothermal treatment of TiO_2 exceeds 170 °C, the formation of titanate nanofibers occurs with an axis of vector [001] [29]. It has been reported that titanate nanofibers had an obvious impact for various applications such as photocatalysis [30] and lithium batteries [31]. However, the size of these kinds of 1D anatase TiO_2 nanofibers is too large to offer a sufficient specific surface area. In a comprehensive consideration, the combination with those nanofibers and TiO_2 nanoparticles might give a notable light-scattering effect with little sacrifice of the specific surface area.

Herein, 1D single-crystalline anatase TiO_2 nanorods (TiO_2-SANRs) were prepared by a simple solvothermal method. The obtained samples were characterized by scanning electron microscopy (SEM), transmission electron microscopy (TEM), and X-ray diffraction (XRD) to elucidate the morphologies, structures, and surface crystal plane. To study the photovoltaic performance of TiO_2-SANRs decorated Degussa P25 nanoparticle solar cells based on different mass ratio of TiO_2-SANRs (0, 10, 20, and 30 wt %), the photocurrent–photovoltage (*J*–*V*) characteristics under AM 1.5G illumination (100 mW/cm^{-2}) and incident photon-to-current conversion efficiency (IPCE) were employed. Moreover, dye-loading of the electrodes and UV–vis reflectance spectra were analyzed in order to discuss the impacts of TiO_2-SANRs and elucidate the origin of the photocurrent enhancement.

EXPERIMENTAL

Materials and reagents

All solvents and reagents, unless otherwise stated, were of analytical quality and used as received. P25 (with a diameter of 20–30 nm) was from Degussa AG (Germany). Tetrabutyl titanate (TBT) was from Aladdin Chemistry Co. Ltd. (China). *N*-methylbenzimidazole (NMBI) and guanidinium thiocyanate (GNCS) were from Aldrich (USA). 1,2-Dimethyl-3-propylimidazolium iodide (DMPII) was bought from Merck AG (Germany), N719 dye ($[(C_4H_9)_4N]_2[Ru(II)L_2(NCS)_2]$, where L = 2,2'-bipyridyl-4,4'-dicarboxylic acid, ruthenium TBA535, Solaronix, Switzerland) were used without further purification.

Conducting glass plates (F: SnO_2 conducting glass, sheet resistance 15Ω/square, Nippon Sheet Glass Co. Ltd, Japan) were used as substrates for screen-printing TiO_2 porous films.

Preparation of TiO_2-SANRs

TiO_2-SANRs were prepared by a facile solvothermal method. Briefly, deionized water (5 mL), anhydrous ethanol (30 mL), and NaOH (0.8 g) were mixed in a 50 mL Teflon-lined stainless steel autoclave. The mixture was stirred for 15 min before the addition of TBT (1.5 mL). The mixture was stirred for another 15 min at room temperature, kept at 180 °C for 12 h. After solvothermal reaction, the precipitates were collected and centrifuged twice with hydrochloric acid (37 % mass fraction), then washed three times with deionized water and ethanol. The subsequent products were dried in an oven at 70 °C (sample a), and then sintered at 500 °C for 30 min (sample b).

Characterization

The crystalline structure of the as-prepared TiO_2-SANRs was examined by a Bruker D8 Advance X-ray diffractometer (XRD) using Cu Kα radiation (1.5406 Å) of 40 kV and 40 mA. Morphological and lattice structural information was investigated by field-emission scanning electron microscopy (FESEM, LEO 1530, Germany), TEM (JEOL 2011, Japan). The adsorbed dye amount was determined by UV–vis absorption, recorded with a spectrophotometer (UV-4802, Unico, USA) with the dye dissolved in a 0.01 M aqueous NaOH solution. Diffuse reflection spectra of the resulting electrodes were collected on a UV–vis–NIR spectrophotometer (UV-3310, Shimadzu Co., Japan) with an integrating sphere.

Device fabrication

The prepared TiO_2-SANRs were used to make the screen-printing paste by mixing with P25 for fabricating the nanocrystalline electrode in DSCs. Mass ratio of the as-prepared TiO_2-SANRs mixed with P25 powder were 10, 20, and 30 wt %. Reference P25 paste was also prepared for comparison. The thickness of the resultant electrodes was controlled by the successive printing times, which was measured by a step profiler (XP-1, MTS, USA). Sealed devices were fabricated according to our previous reports [32] with an active area of 0.16 cm^2. The composition of electrolytes was 1.0 M DMPII, 0.05 M I_2, 0.5 M NMBI, and 0.1 M GNCS in acetonitrile solvent.

Photovoltaic characterization of DSCs

The *J–V* characteristics of DSCs were obtained under AM 1.5G illumination (100 $mW/cm^{-2)}$, realized by a solar simulator (91192, Oriel, USA). The *J–V* curves were measured by applying an external bias voltage to the cell and measuring the generated photocurrent with a digital source meter (Keithley 2400, Keithley Instruments, USA).The incident light intensity was calibrated with a standard crystalline silicon solar cell. IPCE was measured as an action spectrum using IPCE measurement apparatus (PEC-S20, Peccell Technologies, Inc., Japan).

RESULTS AND DISCUSSIONS

Figure 1 presents the XRD patterns for sample a (dried in an oven at 70 °C after acid treatment) and sample b (sample a sintered at 500 °C for 30 min). All the diffraction peaks of sample a in Fig. 1 could be indexed to the crystal structure of $H_2Ti_2O_5{\cdot}H_2O$ (JCPDS 47-0124). And the diffraction peaks of sample b obtained by calcination of $H_2Ti_2O_5{\cdot}H_2O$ at 500 °C for 30 min matched well with the crystal structure of anatase TiO_2 (JCPDS 21-1272).

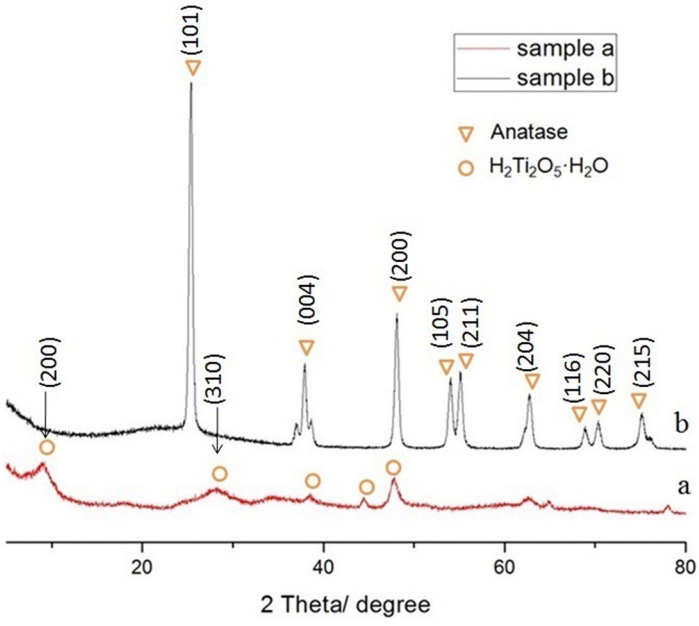

Fig. 1 The XRD patterns of sample a (solvothermal reaction products dried in an oven at 70 °C after acid treatment) and sample b (sample a sintered at 500 °C for 30 min).

Figure 2A shows images of sample a, depicting a morphology of nanorods with a width of 0.5–2 µm and a length up to number of micrometers. In addition, it formed 3D branches near the tip of the nanorods as shown in Fig. 2A, which was caused by ion-exchange thorough the acid treatment. After calcinations, sample b turned to be a cuboid-like nanorod (Fig. 2B), with a diameter between 200–500 nm and length up to a number of micrometers, exfoliated from sample a due to the dehydration and crystal transformation in calcinations [31].

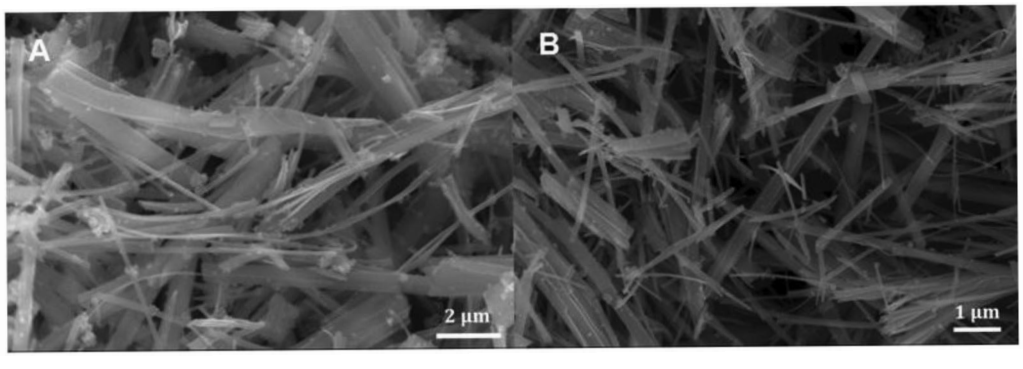

Fig. 2 SEM images of sample a (products dried in an oven at 70 °C after acid treatment) (A), and sample b (sample a sintered at 500 °C for 30 min) (B).

Figure 3 shows the TEM image (A) and high-resolution (HR) TEM image (B) of sample b. Inset of (A) shows a schematic crystallographic structure of sample b. In Fig. 3B, the lattice fringe spacing of 0.358 nm could be assigned to (100) planes of anatase TiO_2, from which the [100] crystal orientation of the single-crystal nanorod could be identified. In Fig. 3C, the lattice fringe spacing of 0.474 nm

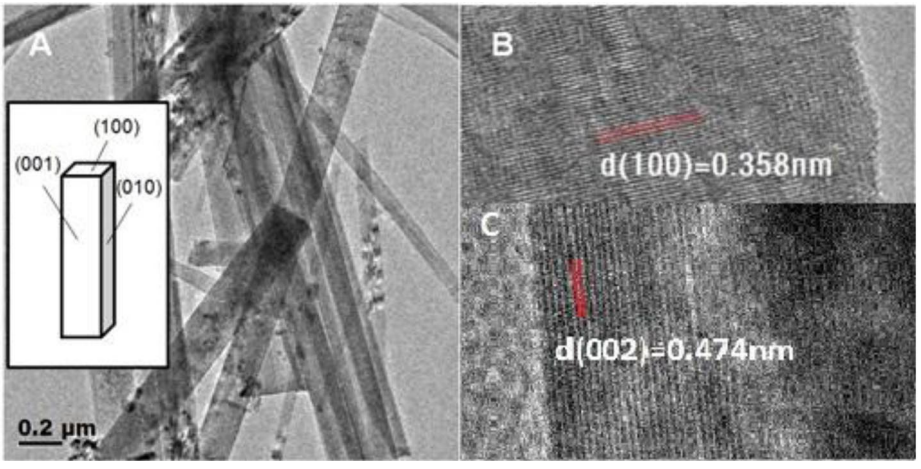

Fig. 3 Typical TEM image (A) and HRTEM image (B) and (C) of sample b (products dried in an oven at 70 °C after acid treatment and sintered at 500 °C for 30 min). Inset of (A) shows schematic crystallographic structure of sample b.

could be assigned to (002) planes of anatase TiO_2, from which the other sides of the unit cell could be indexed to (001) and (010) crystal planes. Both theoretical and experimental studies have shown that the (001) and (010) surfaces of anatase TiO_2 are much more reactive than thermodynamically more stable (101) facet, which may be the dominant source of active sites for various applications like photovoltaic cells, photodegradation of organic molecules, and photocatalytic water splitting [33–37]. However, under alkaline conditions, sodium titanates, which have different crystal structure from TiO_2, would be formed during solvothermal process in the first stage, and the crystal morphology would thus be maintained during acid treatment and calcinations. Therefore, TiO_2 with highly reactive (001) and (010) planes is obtained easily after acid treatment and calcinations of sodium titanates [29].

To assess the performance of TiO_2-SANRs as photoanode materials, the as-prepared TiO_2-SANRs powder, ethyl cellulose, and terpineol were homogeneously mixed with a mass ratio of 18:9:73 to make photoanode pastes. The pastes with different mass ratio (10, 20, and 30 wt %) of the as-prepared TiO_2-SANRs mixed with P25 powder were denoted to devices B, C, and D. The pure P25 paste was also prepared (device A) for comparison. Figure 4 shows the *J–V* characteristics plots of different devices under standard illumination conditions (AM 1.5G, 100 mW/cm^{-2}), while the detailed photovoltaic parameters were collected in Table 1. It can be seen in Fig. 4 and Table 1, the photoelectric conversion efficiency of the solar cell prepared by conventional P25 powder was 6.07 % accompanied with a short-circuit photocurrent density (J_{sc}) of 11.75 mA cm^{-2}, an open-circuit photovoltage of 747 mV and a fill factor of 0.694. Impressively, incorporation of the as-synthesized TiO_2-SANRs could obviously enhance the photovoltaic performance, especially the J_{sc}, and it did not reduce the open-circuit voltage, which happened under the incorporation of the rutile TiO_2 nanorods [22]. Device B with 10 wt % of TiO_2-SANRs displayed a photoelectric conversion efficiency of 6.29 % with a J_{sc} of 12.60 mA cm^{-2}. Device C with 20 wt % TiO_2-SANRs exhibited the highest photoelectric conversion efficiency of 6.89 % together with a J_{sc} of 13.31 mA cm^{-2}. Such a 13.5 % enhancement of the efficiency is mainly raised from the promotion of J_{sc}. At the same time, it was noted that with further increase of the mass fraction of TiO_2-SANRs, the photoelectric conversion efficiency of device D, especially the J_{sc}, had an obvious decline.

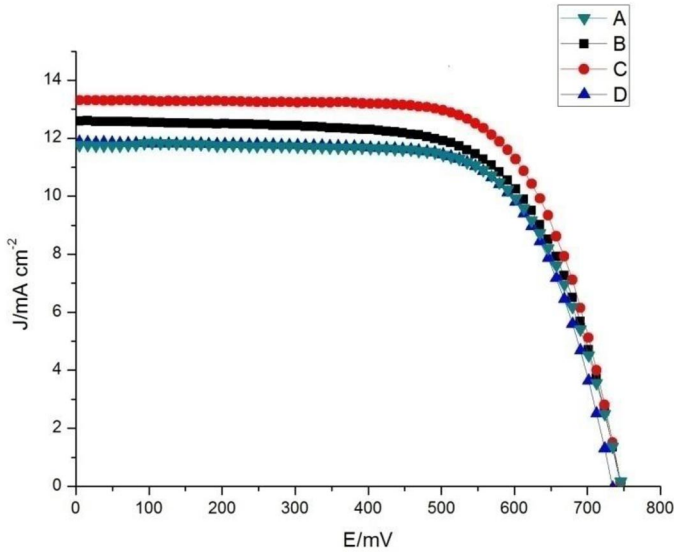

Fig. 4 *I–V* characteristics plots of DSCs based on different mass ratio of TiO_2-SANRs (devices A, B, C, and D corresponding 0, 10, 20, and 30 wt % of TiO_2-SANRs) under one sun illumination (AM 1.5G, 100 mW cm^{-2}).

Table 1 Detailed photovoltaic parameters of DSCs based on different mass ratio of TiO_2-SANRs under one sun illumination (AM 1.5G, 100 mW cm^{-2}).

Devices	Mass ratio of TiO_2-SANRs	Thickness/μm	V_{oc}/mV	J_{sc}/mA cm^{-2}	*FF*	η (%)
A	0 wt %	12.4 ± 0.4	747 ± 2	11.75 ± 0.08	0.694 ± 0.007	6.09 ± 0.03
B	10 wt %	12.7 ± 0.1	745 ± 1	12.60 ± 0.04	0.670 ± 0.009	6.29 ± 0.07
C	20 wt %	12.8 ± 0.2	747 ± 2	13.31 ± 0.05	0.694 ± 0.006	6.89 ± 0.04
D	30 wt %	12.5 ± 0.2	747 ± 1	11.70 ± 0.03	0.700 ± 0.004	6.12 ± 0.04

J_{sc}: short-circuit photocurrent density; V_{oc}: open-circuit photovoltage; η: overall conversion efficiency; *FF*: fill factor.

Furthermore, IPCE response of devices with different mass ratio of the as-synthesized TiO_2-SANRs was analyzed. The IPCE can be expressed as follows:

$$\mathrm{IPCE}(\lambda) = \mathrm{LHE}(\lambda)\phi_{\mathrm{inj}}\eta_{\mathrm{col}} \quad (1)$$

where LHE is the light-harvesting efficiency at a given wave-length, ϕ_{inj} is the quantum yields for electron injection, and η_{col} is the charge collection efficiency [3]. As presented in Fig. 5, it is evident that all spectra show a broad spectral response in the range from 450 to 650 nm, while device C exhibits a significant increase in IPCE response over the long-wavelength range (550–750 nm) compared with the reference P25-based device A.

In order to elucidate the origin of the photocurrent enhancement, the dye-loading of the electrodes was measured by recording the UV–vis absorption spectra of detached dye solutions in 0.01 M NaOH, which are tabulated in Table 2. From the results we can find that with the increasing mass fraction of TiO_2-SANRs, the dye loading has an obvious decrease. This can be easily understood due to the relatively large size of nanorods, which will decrease the specific surface area of the electrode and eventually the dye-loading capacity.

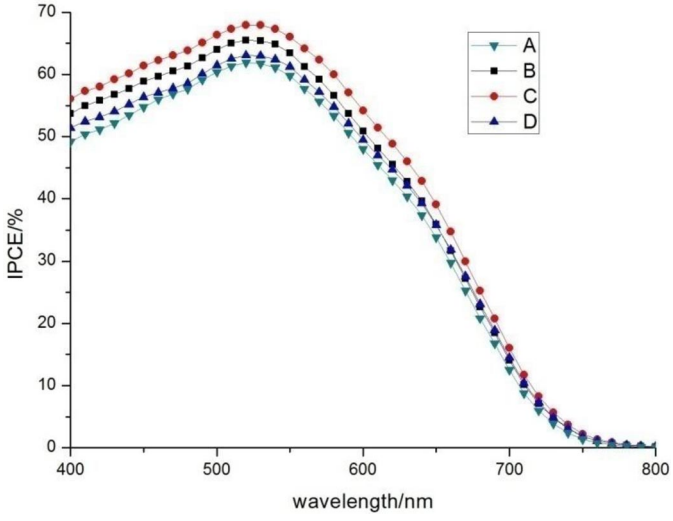

Fig. 5 IPCE spectra of simple devices with different mass ratio of TiO_2-SANRs (devices A, B, C, and D corresponding 0, 10, 20, and 30 wt % of TiO_2-SANRs).

Table 2 Dye-loading capacity and reflectivity at 700 nm^{-1} of devices with different mass ratio of TiO_2-SANRs (devices A, B, C, and D corresponding 0, 10, 20, and 30 wt % of TiO_2-SANRs).

Devices	Dye-loading/mol g^{-1}	Reflectivity at 700 nm^{-1}/%
A	5.56×10^{-5}	20.77
B	5.34×10^{-5}	30.71
C	5.21×10^{-5}	42.65
D	4.99×10^{-5}	47.17

Theoretically, it is proposed that the light-scattering efficiency in a photovoltaic device is greatest when the particle diameter is equal to $k\lambda$, where k is a constant, λ is the wavelength of the incident light. A computer simulation result reported that the optimum particle size for the light-scattering is around 250–300 nm [15].

It should be noticed that there were distinct shoulder peaks in long-wavelength range in the IPCE spectra of samples in conjunction with the as-synthesized TiO_2-SANRs, as shown in Fig. 5, which would be considered as the scattering effect of TiO_2-SANRs. Further analysis for the devices had been realized by using diffuse reflectance spectroscopy. As presented in Fig. 6 and Table 2, the TiO_2-SANRs noticeably improved the light-scattering of DSCs photoanode, which was recognized as the main reason for the J_{sc} enhancement despite the declined dye-loading capacities. For device B, the dye-loading decreased by 7 % compared with device A, while the J_{sc} improved due to the light-scattering effect. Such an improvement of light-scattering became more pronounced especially in long-wavelength range along with the increasing of mass fraction of TiO_2-SANRs. Device C exhibited the highest photoelectric conversion efficiency of 6.89 % accompanied with a J_{sc} of 13.31 mA cm^{-2} compared to 6.09 % and 11.75 mA cm^{-2} for device A. However, further increase of the mass fraction of TiO_2-SANRs to 30 %, the photoelectric conversion efficiency of device D, especially the J_{sc}, had an obvious decline. The light-scattering had a certain increase as shown in Fig. 6; nonetheless, the dye-loading of device D was decreased to 4.99×10^{-5} mol g^{-1}. Therefore, it can be concluded that there exists a notable trade-off between the dye-loading capacity of the electrodes and the light-scattering effects induced by the

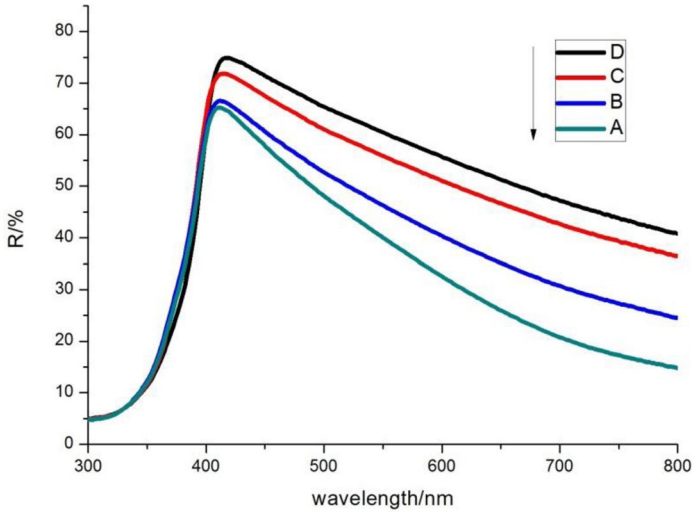

Fig. 6 UV–vis reflectance spectra of devices with different mass ratio of TiO_2-SANRs (devices A, B, C, and D corresponding 0, 10, 20, and 30 wt % of TiO_2-SANRs).

high-aspect-ratio TiO_2-SANRs. Incorporation of such TiO_2-SANRs evokes effect both on the dye-loading and light-scattering performance in the composite electrode, which can be mainly attributed to the relatively large size as well as the high-aspect-ratio of the synthesized TiO_2-SANRs. Therefore, research on the controllable synthesis of the TiO_2-SANRs concurrently featuring efficient dye-loading capacity and light-scattering property needs further attention, which is ongoing work in our laboratory.

CONCLUSIONS

1D TiO_2-SANRs were synthesized through a facile solvothermal method and successfully applied as the photoanodes for efficient DSCs. TiO_2-SANR-decorated Degussa P25 nanoparticle solar cells exhibited 13.3 % enhanced photocurrent density (13.31 mA cm^{-2}) and 13.5 % improved power conversion efficiency (6.89 %) compared with commercial Degussa P25 TiO_2 (P25) solar cells (11.75 mA cm^{-2} and 6.07 %) under standard illumination conditions (AM 1.5G, 100 mW/cm^{-2}). The diffuse reflection spectra showed that the composite photoanodes exhibited obvious light-scattering effect in the long-wavelength region, which can increase the utilization efficiency of the incident light. It was noteworthy that its larger size failed to provide a sufficient specific surface area for the dye-loading, thus endowing a negative role in improving the J_{sc}. Therefore, research on the controllable synthesis of the TiO_2-SANRs concurrently featuring efficient dye-loading capacity and light-scattering property such as hierarchical structure needs further attention, which is an ongoing work in our laboratory.

ACKNOWLEDGMENTS

Financial Supports from the National High Technology Research and Development Program of China (863 Program, 2011AA050522), the Sanjiangyuan Scientific Program of Qinghai Science & Technology Department (2010-N-S03), and the International Cooperation S&T Cooperation Program of China (2010DFA64360) are greatly appreciated.

REFERENCES AND NOTES

1. B. O'Regan, M. Grätzel. *Nature* **353**, 737 (1991).
2. M. Grätzel. *Acc. Chem. Res*. **42**, 1788 (2009).
3. A. Hagfeldt, G. Boschloo, L. Sun, L. Kloo, H. Pettersson. *Chem. Rev*. **110**, 6595 (2010).
4. M. Grätzel. *Nature* **414**, 338 (2001).
5. I. Robel, V. Subramanian, M. Kuno, P. V. Kamat. *J. Am. Chem. Soc*. **128**, 2385 (2006).
6. M. Grätzel. *J. Photochem. Photobiol. C* **4**, 145 (2003).
7. A. Hagfeldt, M. Grätzel. *Chem. Rev*. **95**, 49 (1995).
8. D. Zhao, T. Y. Peng, L. L. Lu, P. Cai, P. Jiang, Z. Q. Bian. *J. Phys. Chem. C* **112**, 8486 (2008).
9. Y. Kondo, H. Yoshikawa, K. Awaga, M. Murayama, T. Mori, K. Sunada, S. Bandow, S. Iijima. *Langmuir* **24**, 547 (2008).
10. H. G. Yang, C. H. Sun, S. Z. Qiao, J. Zou, G. Liu, S. C. Smith, H. M. Cheng, G. Q. Lu. *Nature* **453**, 638 (2008).
11. X. Han, Q. Kuang, M. Jin, Z. Xie, L. Zheng. *J. Am. Chem. Soc.* **131**, 3152 (2009).
12. A. Ghicov, P. Schmuki. *Chem. Commun.* 2791 (2009).
13. C. J. Barbé, F. Arendse, P. Comte, M. Jirousek, F. Lenzmann, V. Shklover, M. Grätzel. *J. Am. Ceram. Soc.* **80**, 3157 (1997).
14. A. Usami. *Chem. Phys. Lett*. **277**, 105 (1997).
15. J. Ferber, J. Luther. *Sol. Energy Mater. Sol. Cells* **54**, 265 (1998).
16. G. Rothenberger, P. Comte, M. Grätzel. *Sol. Energy Mater. Sol. Cells* **58**, 321 (1999).
17. J. Yu, J. Fan, K. Lv. *Nanoscale* **2**, 2144 (2010).
18. M. K. Nazeeruddin, R. Splivallo, P. Liska, P. Comte, M. Grätzel. *Chem. Commun.* 1456 (2003).
19. B. Tan, Y. Y. Wu. *J. Phys. Chem. B* **110**, 15932 (2006).
20. M. Law, L. E. Greene, J. C. Johnson, R. Saykally, P. Yang. *Nat. Mater.* **4**, 455 (2005).
21. J. Jiu, S. Isoda, F. Wang, M. Adachi. *J. Phys. Chem. B* **110**, 2087 (2006).
22. F. Hao, H. Lin, C. Zhou, Y. Liu, J. Li. *Phys. Chem. Chem. Phys.* **13**, 15918 (2011).
23. B. Liu, E. S. Aydil. *J. Am. Chem. Soc.* **131**, 3985 (2009).
24. T. Kasuga, M. Hiramatsu, A. Hoson, T. Sekino, K. Niihara. *Langmuir* **14**, 3160 (1998).
25. T. Kasuga, M. Hiramatsu, A. Hoson, T. Sekino, K. Niihara. *Adv. Mater.* **11**, 1307 (1999).
26. Y. Lan, X. Gao, H. Zhu, Z. Zheng, T. Yan, F. Wu, S. P. Ringer, D. Song. *Adv. Funct. Mater*. **15**, 1310 (2005).
27. X. Meng, D. Wang, J. Liu, S. Zhan. *Mater. Res. Bull.* **39**, 2163 (2004).
28. D. V. Bavykin, J. M. Friedrich, Frank C. Walsh. *Adv. Mater*. **18**, 2807 (2006).
29. Z. Yuan, B. Su. *Colloids Surf., A* **241**, 173 (2004).
30. W. Li, Y. Bai, W. Liu, C. Liu, Z. Yang, X. Feng, X. Lu, K.-Y. Chan. *J. Mater. Chem.* **21**, 6718 (2011).
31. L. Kavan, M. Kalbac, M. Zukalova, I. Exnar, V. Lorenzen, R. Nesper, M. Grätzel. *Chem. Mater.* **16**, 477 (2004).
32. F. Hao, H. Lin, J. Zhang, D. Zhuang, Y. Liu, J. Li. *Electrochim. Acta* **55**, 7225 (2010).
33. G. S. Herman, Z. Dohnalek, N. Ruzycki, U. Diebold. *J. Phys. Chem. B* **107**, 2788 (2003).
34. A. Vittadini, A. Selloni, F. P. Rotzinger, M. Grätzel. *Phys. Rev. Lett.* **81**, 2954 (1998).
35. X. Wu, Z. Chen, G. Q. Lu, L. Wang. *Adv. Funct. Mater.* **21**, 4167 (2011).
36. M. Lazzeri, A. Vittadini, A. Selloni. *Phys. Rev. B* **63**, 155409 (2001).
37. W. Yang, Y. Wang, W. Shi. *CrystEngComm* **14**, 230 (2012).

